ISSN 0915-633X

NATIONAL INSTITUTE FOR FUSION SCIENCE

Observation of the Limit Cycle in the Asymmetric Plasma Divided by the Magnetic Filter

K. Ohi, H. Naitou, Y. Tauchi and O. Fukumasa

(Received - July 10, 2000)

NIFS-640 Aug. 2000

RESEARCH REPORT
NIFS Series

NAGOYA, JAPAN

Observation of the Limit Cycle in the Asymmetric Plasma Divided by the Magnetic Filter

K Ohi, H. Naitou*, Y. Tauchi, O. Fukumasa

Department of Electrical and Electronic Engineering,
Yamaguchi University, Tokiwadai 2-16-1, Ube 755-8611, Japan

Abstract

An asymmetric plasma divided by the magnetic filter (MF) is numerically simulated by the one-dimensional particle-in-cell code VSIM1D. Depending on the asymmetry, the system behaves static or dynamic. In the static state, the potentials of the main plasma and the subplasma are given by the sheath potentials, $\phi_M \sim 3T_{Me}/e$ and $\phi_S \sim 3T_{Se}/e$, respectively, with e being an electron charge and T_{Me} and T_{Se} being electron temperatures ($T_{Me} > T_{Se}$). In the dynamic state, while $\phi_M \sim 3T_{Me}/e$, ϕ_S oscillates periodically between $\phi_{S\,min} \sim 3T_{Se}/e$ and $\phi_{S\,max} \sim 3T_{Me}/e$. The ions accelerated by the time varying potential gap get into the subplasma and excite the laminar shock waves. This periodic phenomenon can be understood as a limit cycle due to transitions between two bifurcated states of $\phi_{S,min}$ and $\phi_{S,max}$.

Keywords: magnetic filter, laminar shock wave, limit cycle, particle simulation, PIC code, bifurcation

1 Introduction

The magnetic filter (MF) is a localized magnetic field, which can divide a plasma into two regions of different parameters. In the volume negative hydrogen/deuterium ion source, for example, the MF is the critical component to isolate a diffused plasma from a source plasma. The major mechanism to create negative hydrogen/deuterium ions is the two step process of the vibrational excitation and the dissociative attachment[1, 2]. The source plasma involves fast electrons with energies in excess of $20 - 30$ eV to produce molecules of highly vibrationally excited states. These excited molecules can travel to the diffused plasma across the MF, while high energy electrons are reflected by the MF. The diffused plasma, hence, includes only low energy electrons with the temperature of about 1 eV which are necessary for the dissociative attachment to the vibrationally excited molecules. This sort of "double plasma" configuration might be useful for the processing plasma: the plasma with energetic electrons and the low temperature plasma without energetic electrons are needed for the production of radical species and for the reduction of the harmful energetic ion bombardment (due to the sheath potential) to the substrate surface, respectively[3].

There are three effects of the MF. The first and primary effect is the Lorentz force on electrons and ions. Depending on the mass and the energy of charged particles, the action of the MF is different for individual particles. The MF, hence, works as the filter to select particles which can go through the MF. The second is the diffusion process of the charged particles. Collisional and/or the turbulent transports across the MF can explain the character of the MF in which energetic electrons diffuse much slower than the low energy electrons. The turbulent diffusion is due to $\boldsymbol{E}\times\boldsymbol{B}$ drifts with $\boldsymbol{E}$ being the fluctuating electrostatic electric field and $\boldsymbol{B}$ being the static magnetic field of the MF; the finite gyroradious effects of electrons elucidate the slow random walks of energetic electrons because high energy electrons average out the fine scale fluctuations of the electric field [4, 5, 6]. The third is the formation of the potential gap between two regions separated by the MF. This potential gap made by the first and second effects acts as the electrostatic filter on electrons and ions.

In order to understand the complex behavior of the plasma with the MF, particle-in-cell (PIC) simulations have been executed. The transport process and the potential formation of the plasma divided by the MF have been investigated by the two-dimensional particle simulation[5, 6, 7, 8]. We have believed in the existence of the static state with the equilibrium density, temperature, and space potential profiles. So our concern was limited to the understanding of the transport process due to the fluctuating turbulent electrostatic field around the MF. Recently, we have unexpectedly found the non-static dynamic state in the plasma with the MF[9] by executing the one-dimensional PIC simulation with a newly developed VSIM1D code[10] (Visualized particle SIMulation code in 1-Dimension) which runs on PC-UNIX operating system and displays the real time portrayal of the phase space plots of charged parti-

*Guest staff of National Institute for Fusion Science, Toki, Gifu 509-5292, Japan (April 1 1999 - March 31 2001)

cles and the potential profile etc. on the monitor. The limit cycle in the terminology of the nonlinear physics is observed. The periodic variation of the potential gap and the periodic excitation of the laminar shock waves[11] caused by ions accelerated by the potential gap constitute the physics underling the limit cycle. The movies of the temporal evolutions of the potential profiles and the phase space plots of ions can be found on the CD-ROM compiled in Ref.12. This article extends the study of the previous paper[9] in which only the discovery of the dynamic state with a brief physical discussion was reported. Simulations using a doubled system size with various parameters are done to verify the generality of the previous results. Detailed measurements are added to clear the physical picture of the phenomena. Also the parameter range in which the system behaves dynamic is studied carefully.

This paper is organized as follows. The basic simulation model of the asymmetric plasma with the MF is described in Sec.2. Simulation results are presented in Sec.3. Conclusions and the discussion are given in Sec.4.

2 Simulation Model

The one-dimensional particle-in-cell code VSIM1D[10] is used for the simulation of the asymmetric plasma divided by the MF. Physical quantities are allowed to change only in the x-direction. Hydrogen plasma is assumed. Full dynamics of electrons and ions are followed under the electrostatic approximation. A schematic diagram of the simulation model is depicted in Fig.1. Left and right ends of the system, $x = 0$ and $x = L_x$, are grounded walls. Particles hitting the walls are absorbed there. Ion sheaths, hence, will be formed next to the walls. There is a MF at the center of the system ($x = x_{MF}$) and the direction of the magnetic field is in the z-direction. The spatial profile of the magnetic field strength is given by

$$B(x) = B_0 \exp[\, -0.5(x - x_{MF})^2/a_{MF}^2 \,] \,.$$

where B_0 is the maximum magnetic field strength and a_{MF} is the characteristic width of the MF. The strength of the MF is chosen to influence only electron dynamics; ions move freely across the MF. To the right of the MF, there is a high temperature and high density main plasma. A low temperature and low density subplasma exists to the left of the MF. The source regions are located in the main plasma and the subplasma, respectively, to produce new electrons and ions which will equal the particle loss to the walls.

The physical quantities in this article are expressed in the normalized units. The length is normalized by the grid size Δ. The time is normalized by the inverse of the electron plasma angular frequency ω_{pe}^{-1}, where $\omega_{pe} = (n_{e0}e^2/\epsilon_0 m_e)^{1/2}$ is defined by the initial average electron density ($n_{e0} = n_{i0} = n_0$) in the main plasma, e and m_e are the charge and the mass of electrons, and ϵ_0 is the permittivity in vacuum. Temperatures and potentials are normalized by $m_e\Delta^2\omega_{pe}^2$ and $m_e\Delta^2\omega_{pe}^2/e$, respectively. Note that temperatures in this article are expressed in the energy unit. The normalized strength of B_0 equals to ω_{ce}/ω_{pe} ($\omega_{ce} = eB_0/m_e$ is the electron cyclotron angular frequency at $x = x_{MF}$). Simulation parameters are as follows: system size: $L_x = 400$, $x_{MF} = 200$, $a_{MF} = 12$, $B_0 = 0.2$ - 1.0, electron Debye length in the main plasma: $\lambda_{de} = 2$, mass ratio: $m_i/m_e = 1836$, time step size: $\Delta t = 0.2$, total number of time steps: $N_t = 400{,}000$. Hereafter, we will add subscripts M and S for the quantities related to the main plasma and the subplasma, respectively. The initial electron temperatures of the respective plasmas are $T_{Me} = 4$ and $T_{Se} = 1$. The initial ion temperatures are set to be $T_{Mi} = T_{Si} = 0.4$. The initial electron density of the subplasma is one forth of the density of the main plasma. Initial ion density profile is the same as that of electrons. Note that initial conditions are not so important in this simulation because the system includes particle source and loss and our concern is the long time behavior.

In order to make up for the particle loss from the respective regions, electrons and ions are injected constantly into the source regions. In the main plasma, one electron and one ion are injected every one time step with given temperatures of $T_{Me} = 4$ and $T_{Mi} = 0.4$ in the region of $220 < x < 380$. In the subplasma, one electron and one ion are inserted every N_{in} time steps with $T_{Se} = 1$ and $T_{Si} = 0.4$ in the region of $20 < x < 180$. N_{in} is varied between 8 and 256. In the source regions, the artifical 'thermalization' is done; velocity distributions of electrons in the respective source regions are reset to form new Maxwellian distributions every 150 time steps. Without this process, the electron velocity distributions would be cooled eventually because only low energy electrons are confined in the system by the sheath potential near the walls. The total number of particles used in this simulation for each species is about thirty thousands. The total running time is about 12 hours on the PC/AT compatible personal computer using the CPU of Celeron 450 MHz.

3 Simulation Results

Before presenting the simulation results for the dynamic state, let us consider the static state. It is easy to predict that there are two types of the static equilibrium potential profile for the asymmetric plasma divided by the MF. The first is corresponding to the case in which effects of ions coming form the main plasma to the subplasma is negligible. Each plasma has the space potential of the order of the electron temperature ($\phi \sim 3T_e$) which is equal to the sheath potential adjacent to the respective grounded wall. The space potential of the main plasma is higher than that of the subplasma since $T_{Me} > T_{Se}$. The example of this case is shown in Figs.2 and 3. The parameters

chosen for this case are $B_0 = 0.7$ and $N_{in} = 64$. It is found that the system approaches the static state after $t \sim 20000$. Fig 2 represents the time evolutions of the average electron densities in the main plasma and the subplasma. The average electron densities are measured in the source regions of the respective zones. In the stationary state, the average electron density in the main plasma is $< n_{Me} > \simeq 1.66 n_0$, while that in the subplasma is $< n_{Se} > \simeq 0.12 n_0$. The density ratio $< n_{Se} > / < n_{Me} > \simeq 0.072$ is much larger than the ratio of the particle supplement, $1/N_{in} \simeq 0.016$. The improved electron confinement in the subplasma is explained by the ions coming from the main plasma. Fig.3 depicts the time evolutions of the potentials of the main plasma and the subplasma. φ_M and φ_S, measured at the centers of the respective regions. These potentials are time averaged over $\tau = 20$ to eliminate the fluctuating noise concerning electron plasma oscillations. The potential gap between φ_M and φ_S is observed. The measured potentials, φ_M and φ_S, are equal to the sheath potential next to the grounded walls, $\sim 3T_{Me}$ and $\sim 3T_{Se}$, respectively. The deviation of φ from the average value is determined by the thermal fluctuations in the respective areas. (We can reduce these fluctuations by drastically increasing the number of particles in the simulation with the expense of computer resources.) It is to be noticed that the potential gap at the MF accelerates ions in the main plasma into the subplasma; there is an ion beam component in the subplasma. No instability is observed due to the ion beam component in this static case.

The second static case will be found when the effects of ions intruding into the subplasma across the MF is dominant. Electrons in the subplasma cannot keep the space potential from going up by reducing the electron loss to the wall. Therefore, the potential of the subplasma is a little bit higher than that of the main plasma, while the potential of the main plasma is determined by the electron temperature: $\varphi_M \sim 3T_{Me}$ and $\varphi_S \sim 3T_{Me} + 3T_{Mi} \sim 3T_{Me}$ since $T_{Mi} \ll T_{Me}$. (In this case, electrons in the subplasma is confined very well by the sheath potential. Hence, in the strict sense, to maintain the stationary state, loss mechanism of electrons in the subplasma must be taken into account.)

We have found that there is a dynamic state in which the potential in the subplasma oscillates periodically between values of $\sim 3T_{Me}$ and $\sim 3T_{Se}$. The example of this dynamic state is shown in Figs.4 and 5. The parameters chosen for this case are $B_0 = 0.5$ and $N_{in} = 64$. Fig 4 expresses the time evolutions of the average electron densities in the main plasma and the subplasma. We can see the periodic oscillations in the ripples of the average densities in the respective regions after $t \sim 8000$. The system approaches the stationary state after $t \sim 30000$. The period of the oscillations of the ripples is about 2000. In the stationary state, $< n_{Me} > \simeq 1.56 n_0$ and $< n_{Se} > \simeq 0.15 n_0$ with $\Delta < n_{Me} > \simeq \Delta < n_{Se} > \simeq 0.032 n_0$ where $\Delta < n_{Me} >$ and $\Delta < n_{Se} >$ indicate the heights of the density ripples. The density ratio is $< n_{Se} > / < n_{Me} > \simeq 0.096$. Fig 5 depicts the time evolutions of the potentials at the centers of the main plasma and the subplasma. The potential of the main plasma is almost constant ($\varphi_M \sim 12$) with small ripples, while that of the subplasma oscillates between $\varphi_S \sim 3$ and $\varphi_S \sim 12$. The period of the potential oscillation in the subplasma equals to that of the density ripples.

To understand the physical mechanism of the dynamic state, detailed measurements were done concentrating on the case of $B_0 = 0.5$ and $N_{in} = 64$. Typical four periods of the time variations of the average electron densities are extracted from Fig 4 and shown in Fig 6. Note that the axes in Fig.6 are different for $< n_{Me} >$ and $< n_{Se} >$ in the offsets of the scales. It is clear that $< n_{Se} >$ increases (decreases) when $< n_{Me} >$ decreases (increases) with the delay time of $\tau_D \sim 500$. The delay time is caused by the space between source regions since $< n_{Me} >$ and $< n_{Se} >$ are the average densities of the respective source regions. The ions going out of the source region in the main plasma cross the domain of the MF and come to the source region of the subplasma after the time of l/v_{Di}, where $l = 40$ is the space between the source regions and v_{Di} is the average drift speed of ions crossing the MF. We can estimate $v_{Di} \sim l/\tau_D \sim 0.08$ which is almost the same as the ion drift speed of $v_{Di} \sim 0.1$ given by the normalized equation for the energy conservation

$$\frac{1}{2} m_i v_{Di}^2 \sim \varphi_M - \varphi_S ,$$

where we used $\varphi_M \sim 12$, $\varphi_S \sim 3$, and $m_i = 1836$.

Typical four periods of the time evolutions of φ_M and φ_S are extracted from Fig.5 and depicted in Fig.7. The time scales for Figs.6 and 7 are the same. We can see that the phase of φ_S is synchronized with that of the density ripple of $< n_{Se} >$, although there is a slight difference in the wave forms of φ_S and $< n_{Se} >$. When φ_S is at the minimum, the ion flux from the main plasma increases due to the potential gap between the main plasma and the subplasma. Then the ion density in the subplasma increases; $< n_{Se} >$ also enhances due to quasineutrality. When φ_S is at the maximum, the ion flux from the main plasma is small since there is no potential gap. The part of the slow increase of $< n_{Se} >$ after the fast increase may be explained by the particle supplement in the source region and the good electron confinement due to the large sheath potential at the left wall. As will be shown later, when the potential gap is maximum, the higher energy ion beam with the higher density gets into the subplasma. φ_S and $< n_{Se} >$ reduce when these energetic ions get out of the system. The same process continues periodically.

The snap shots of phase space plots of ions (top), ion density profiles (middle), and potential profiles (bottom) are shown in Fig.8 for different time steps in one period. Four different times in Fig.8 are depicted in Figs.6, 7 and 9 by the arrows with the alphabets of (a), (b), (c), and (d). In the phase space plots,

red points indicate ions generated in the main plasma, whereas blue points denote ions introduced in the subplasma. Hence the red points in the subplasma show ions coming from the main plasma. We can see the structure in the ion density profile in the subplasma. In the density profile, there is a peak moving in the negative x direction. Arrows in Fig.8 show the positions of the density peaks. The structure of the ion density reflects the phase space dynamics of the ion beam accelerated by the potential gap and traveling in the subplasma. We can also see slight peaks of the electrostatic potential profile at the same positions of the density peaks in the subplasma. The period of the limit cycle is determined by the transit time of the faster ions accelerated when the potential gap is maximum.

In the former paper[9], we called the collective phenomena induced by the ion beam as the beam instability. Lately we recognized that we are observing the laminar shock waves generated by the modulated ion beam. The linear two stream instability is stable for our case. The phenomenon is very close to the one experimentally observed by H. Ikezi et al.[11]. They used a double plasma device in which the energy of the ion beam coming into the low density target plasma is suddenly increased at some time. The faster ions overtake the slower ions and the shock wave structure is formed. The change of energy in the experiment of Ikezi et al. corresponds to the variation of the potential gap in our case. Both cases are similar in the two facts: (1) A significant amount of ions is reflected from and transmitted through the shock front. (2) The width of the shock increases in time. These facts are clearly observed in the phase space plots in Fig.8. The behavior of the system in one period of the oscillation is summarized in the following. When the potential gap is large, the ion beam flux from the main plasma is large and forms the shock wave structure due to the overtaking of the slower ions by the faster ions (see Fig.8 (a)). As the results of the higher ion beam flux the potential of the subplasma increases to the level of the potential of the main plasma (Fig.8 (b), (c)). In this time scale the ion beam flux from the main plasma reduces as the potential gap decreases. At the time when the head of the shock wave structure reaches the left wall, the potential in the subplasma starts to decrease (Fig.8 (d)). When the old shock wave goes out of the system, the ions with the higher speed and the higher density come into the subplasma and excite the new shock wave: this process continues periodically.

The speed of the ion sound wave in our simulation is $c_s = \sqrt{(T_e + 3T_i)/M_i} \simeq 0.035$. From the phase space plots of Fig.8 (a) we see that the velocities before and behind the shock wave structure are $v_{min} \simeq 0.060$ and $v_{max} \simeq 0.094$, respectively. The velocities of the head and the tail of the shock wave structure are calculated from the sixteen snap shots of the ion density profile in one period. The velocity of the head of the shock wave structure is $v_H \simeq 0.096$, while the velocity of the tail of the shock wave is $v_T \simeq 0.053$. Hence, the width of the shock wave structure increases in time. Note that the arrows in Fig.8 designate the positions of the tails of the shock wave structures. The ion density between the head and the tail of the shock wave structure is higher than that of the ambient plasma. We can think of these head and tail of the shock wave structure as two shock fronts: in the frame moving with the average ion velocity, we have two shock waves propagating forward and backward directions. Mach number of the faster shock (head) is $(v_H - v_{min})/c_s \simeq 1.0$, while that of the slower shock (tail) is $(v_{max} - v_T)/c_s \simeq 1.2$. The difference in Mach number may explain why the tail of the shock wave structure is more prominent than the head. Mach number of the head becomes subsonic in time: then the shock wave structure around the head disappears (see Fig.8(c) and (d)).

The time evolution of the ion density at the center of the subplasma is shown in Fig.9 for four periods of the limit cycle. The time scale of this figure is the same as those of Figs.6 and 7. The sharp peaks in the figure correspond to the passage of the tail of the shock wave structure. The sudden reduction of the ion density just after the maximum is followed by the slow decrease. Considering that the ion density displayed in the figure is the sum of the background ions born in the subplasma and the ions coming from the main plasma, the amount of the ions coming from the main plasma is an order of magnitude larger than that of the background ions in the subplasma.

To identify the parameter range in which the asymmetric plasma with the MF behaves dynamic, simulations with different values of N_{in} and B_0 are done. Fig.10 depicts the average electron density in the subplasma $< n_{Se} >$ depending on the rate of the particle supplement in the subplasma, $1/N_{in}$. The strength of the MF is fixed at $B_0 = 0.5$. For $B_0 = 0.5$, the electrons in the main plasma and the subplasma cannot commute each other. The maximum and minimum values are shown in the figure. The cases with the same values of maximums and minimums correspond to the static states. The dynamic state of the limit cycle is observed for $1/N_{in} \leq 0.05$, while the static state is seen for $1/N_{in} \geq 0.0625$. It is natural that if the background electron density is small (*i.e.*, $1/N_{in}$ is small) the loss of high energy electrons into the left wall cannot prevent the increase of the space potential of the subplasma from increasing up to the level of ϕ_M when certain amount of ions enter the subplasma. Hence the dynamic state manifests for the low value of $1/N_{in}$. The periods of the limit cycles are the same for all cases with $1/N_{in} \leq 0.05$.

Fig.11 shows the average electron density in the subplasma, $< n_{Se} >$, depending on B_0. The parameter of $N_{in} = 64$ is fixed. For the stronger magnetic field of $B_0 \geq 0.65$, the static state with the potential gap is observed. Although there is no communication of electrons between the main plasma and the subplasma for $B_0 \gtrsim 0.5$, the electron density at the MF is determined by the electrons coming from the main plasma or the subplasma. The penetration length of

electrons into the region of the MF is roughly determined by the Larmor radius, hence the electron density at the MF is a decreasing function of B_0. Due to the quasineutrality, the ion density at the MF is also a decreasing function of B_0: the ion flux from the main plasma to the subplasma reduces as B_0 increases. So, for the larger value of B_0, the ion beam from the main plasma does not have enough power to cause the potential increase in the subplasma. For the weaker magnetic field of $B_0 \leq 0.35$, the static states with $\phi_S \sim 3$ and $\phi_M \sim 12$ are observed again. For these lower values of B_0, energetic electrons in the main plasma pass the MF, lose energy due to the potential gap, and enter into the subplasma. So the electron density in the subplasma increases. The increased number of electrons in the subplasma has the function to keep the sheath potential at the level of $\phi_S \sim 3$.

We observe the dynamic state for $0.4 \leq B_0 \leq 0.6$. For $B_0 = 0.5$, 0.55, and 0.6, the system shows the limit cycle. For the relatively weak values of $B_0 = 0.4$ and 0.45, the intermittent states manifest. In the intermittent cases, some of electrons from the main plasma can go to the subplasma and affects the potential change in the subplasma. The study of these intermittent states is outside the scope of this article and will be the subject of a future article.

4 Conclusions and Discussion

The asymmetric plasma divided by the magnetic filter (MF) is numerically simulated by the one-dimensional particle-in-cell code VSIM1D. The strength of the MF is chosen to influence only electron dynamics: ions move freely across the MF. The main plasma with the high temperature (T_{Me}) and the high density faces the subplasma with the low temperature (T_{Se}) and the low density across the MF located at the center of the system. The particles hitting the grounded walls at the left and right ends of the system are absorbed there: there are ion sheaths adjacent to the walls. Depending on the asymmetry, the system behaves static or dynamic. In the static state, the potentials of the main plasma and the subplasma are given by the sheath potentials, $\phi_M \sim 3T_{Me}$ and $\phi_S \sim 3T_{Se}$, respectively. In the dynamic state, while the potential in the main plasma is almost constant with $\phi_M \sim 3T_{Me}$, the potential in the subplasma oscillates periodically between $\phi_{S,min} \sim 3T_{Se}$ and $\phi_{S\,max} \sim 3T_{Me}$. When the potential gap between the main plasma and the subplasma is maximum, the ion beam with the higher speed and the higher density gets into the subplasma from the main plasma. Then the potential in the subplasma increases gradually because of the increased ion beam flux from the main plasma. The ion beam with the higher speed excites the laminar shock wave when it travels in the subplasma. When the shock wave structure is absorbed into the left wall, the space potential of the subplasma becomes small and the new ion beam with the higher speed and the higher density gets into the subplasma across the MF due to the large potential gap. This process continues periodically. The period of the limit cycle is determined by the transit time of ions accelerated when the potential gap is maximum.

The phenomena presented in this article can be understood as the self-sustained oscillation related to the bifurcation of the potential in the subplasma (or the electric field at the MF). The phenomena caused by the transitions between two bifurcated states have been observed in toroidal magnetic fusion devices. One example is the edge localized modes (ELMs) in tokamaks[13]. Dithering ELMs are recognized as the transitions between L-mode and H-mode in which L and H mean low and high confinements, respectively. The experimentally observed dithering ELMs can be elucidated by a limit cycle solution of the Ginzburg-Landau type equation[14]. The other example is a self-sustained oscillation in Compact Helical System (CHS) (helitron / torsatoron device) related to the bifurcation of a radial electric field and the formation of a transport barrier[15]. Sometimes the bifurcated system behaves chaotic or intermittent as in the case of ELMs[16, 17]. We have also observed the dynamic state with intermittency, although the presentation of details will be the subject of a forthcoming paper.

Acknowledgement

The authors would like to express their thanks to Professors T. Kamimura, and K. Itoh, and H. Sanuki, National Institute for Fusion Science, Professor Y. Kawai, Kyushu University, and Professor K. Saeki, Shizuoka University, Professor Y. Ohsawa, Nagoya University for stimulating discussions. This work was supported in part by the Grant-in-Aid for Scientific Research from the Japanese Ministry of Education, Science, Sports and Culture.

References

[1] J. R. Hiskes and A. M. Kano, J. Appl. Phys. **56**, 1927 (1984).

[2] O. Fukumasa, J. Phys. D. **22**, 1668 (1989).

[3] O. Fukumasa, Y. Tauchi, S. Sakiyama, J. Appl. Phys. **36**, 4593 (1997).

[4] H. Naitou, T. Kamimura, J. M. Dawson, J. Phys. Soc. Japan, **46**, 258 (1979).

[5] O. Fukumasa, H. Naitou, S. Sakiyama, J. Appl. Phys. **74**, 848 (1993).

[6] H. Naitou, O. Fukumasa, and K. Sakachou, Rev. Sci. Instrum. **67**, 1149 (1996).

[7] H. Naitou, O. Fukumasa, K. Sakachou, and K. Mutou, Rev. Sci. Instrum. **65**, 1438 (1994).

[8] H. Naitou, O. Fukumasa, K. Sakachou, and K. Mutou, Fusion Engineering and Design, **26**, 523 (1995).

[9] H. Naitou, K. Ohi, O. Fukumasa, Rev. Sci. Instrum. **71**, 875 (2000).

[10] K. Koga, H. Naitou, Y. Kawai, J. Phys. Soc. Japan. **68**, 1578 (1999).

[11] H. Ikezi, T.Kamimura, M. Kako, and K. E. Longren, Phys. Fluids. **16**, 2167 (1973).

[12] H. Naitou, K. Ohi, Y. Tauchi, O. Fukumasa, in ' Virtual Plasma Laboratory: Movie Collection of Plasmas', J. of Plasma and Fusion Res. **76**, 3 (2000).

[13] H. Zohm, Plasma Phys. Control. Fusion, **38**, 105 (1996).

[14] S. -I. Itoh, K. Itoh, A. Fukuyama, Y. Miura and JFT-2M Group, Phys. Rev. lett. **67**, 2485 (1991).

[15] A. Fujisawa, H. Iguchi, H. Idei, S. Kubo, K. Matsuoka, S. Okamura, K. Tanaka, T. Minami, S. Ohdachi, S. Morita, H. Zushi, S. Lee, M. Osakabe, R. Akiyama, Y. Yoshimura, K. Toi, H. Sanuki, K. Itoh, A. Shimizu, S. Takagi, A. Ejiri, C. Takahashi, M. Kojima, S. Hidekuma, K. Ida, S, Nishimura, M. Isobe, N Inoue, R. Sakamoto, S. -I. Itoh, Y. Hamada, and M. Fujiwara, Phys. Rev. lett. **81**, 2256 (1998).

[16] S. -I. Itoh, S. Toda, M. Yagi, K. Itoh, A. Fukuyama, Plasma Phys. Control. Fusion **40**, 737 (1998).

[17] S. Toda, S. -I. Itoh, M. Yagi, K. Itoh, A. Fukuyama, J. Phys. Soc. Jpn., **68**, 3520 (1999).

Figure captions

Fig.1 Schematic diagram of the simulation model with the MF.

Fig.2 Time evolutions of average electron densities in the main plasma and the subplasma, $< n_{Me} >$ and $< n_{Se} >$, for $B_0 = 0.7$ and $N_{in} = 64$.

Fig.3 Time evolutions of potentials at the centers of the main plasma and the subplasma, φ_M and φ_S, for $B_0 = 0.7$ and $N_{in} = 64$.

Fig.4 Time evolutions of average electron densities in the main plasma and the subplasma, $< n_{Me} >$ and $< n_{Se} >$, for $B_0 = 0.5$ and $N_{in} = 64$.

Fig.5 Time evolutions of potentials at the centers of the main plasma and the subplasma, ϕ_M and φ_S, for $B_0 = 0.5$ and $N_{in} = 64$.

Fig.6 Typical four periods of average electron density oscillations of the main plasma and the subplasma, $< n_{Me} >$ and $< n_{Se} >$, for $B_0 = 0.5$ and $N_{in} = 64$.

Fig.7 Typical four periods of potential oscillations at the centers of the main plasma and the subplasma, ϕ_M and ϕ_S, for $B_0 = 0.5$ and $N_{in} = 64$.

Fig.8 Snap shots of phase space plots of ions, ion density profiles, and potential profiles for $B_0 = 0.5$ and $N_{in} = 64$. Time variation for a period is shown.

Fig.9 Typical four periods of the time evolution of the ion density at the center of the subplasma for $B_0 = 0.5$ and $N_{in} = 64$.

Fig.10 Average electron density in the subplasma $< n_{Se} >$ depending on the rate of particle supplement in the subplasma, $1/N_{in}$. The maximum and minimum are shown for the dynamic case.

Fig.11 Average electron density in the subplasma $< n_{Se} >$ depending on B_0. The maximum and minimum are shown for the dynamic case. Data points indicated by L and I correspond to the limit cycles and the intermittent states, respectively.

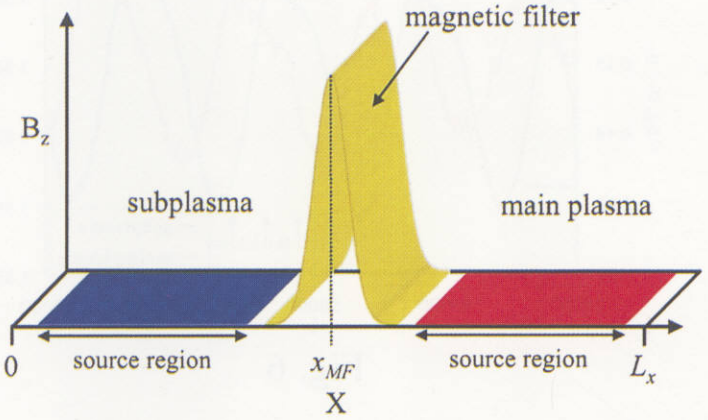

Fig. 1

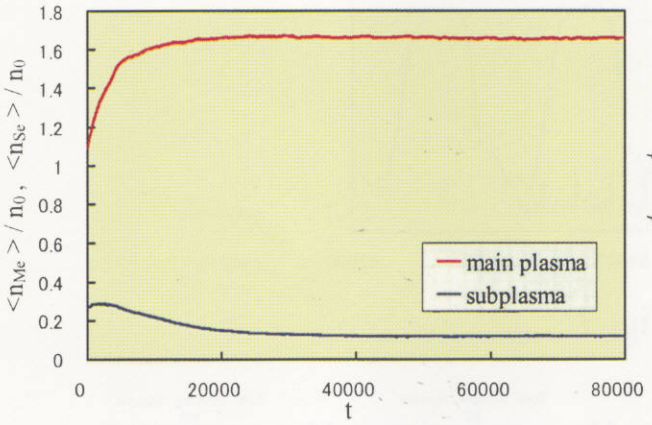

Fig. 2

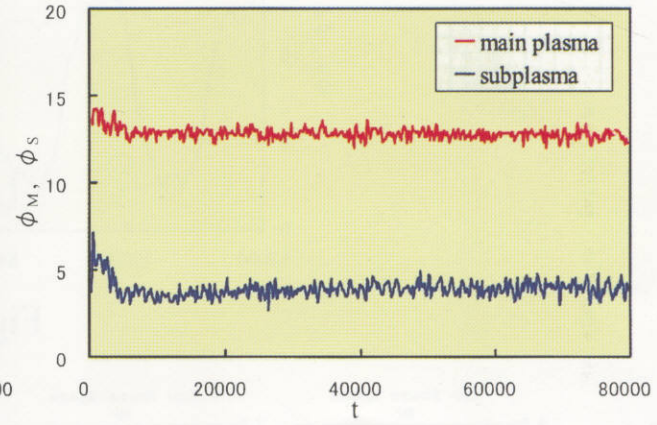

Fig. 3

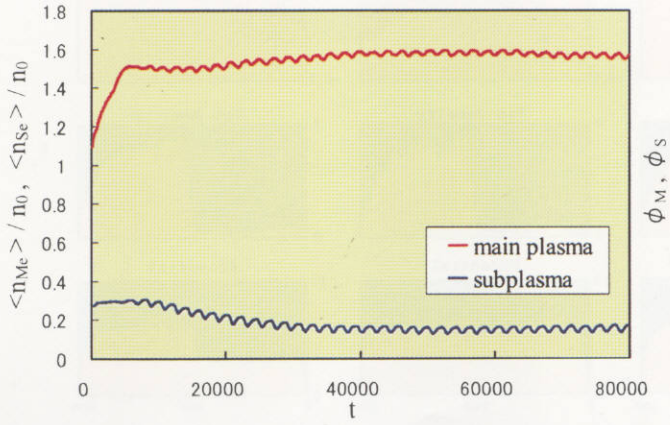

Fig. 4

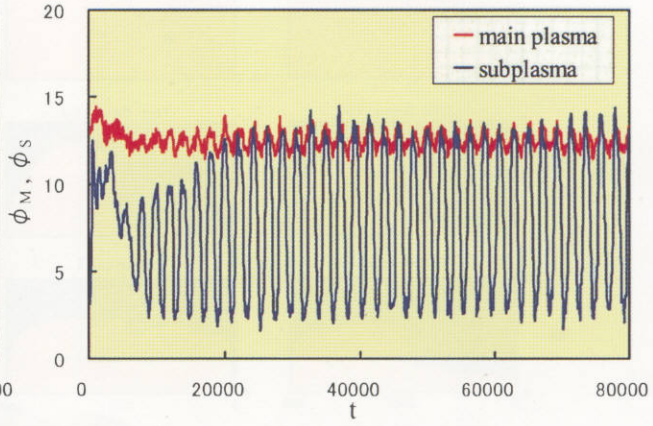

Fig. 5

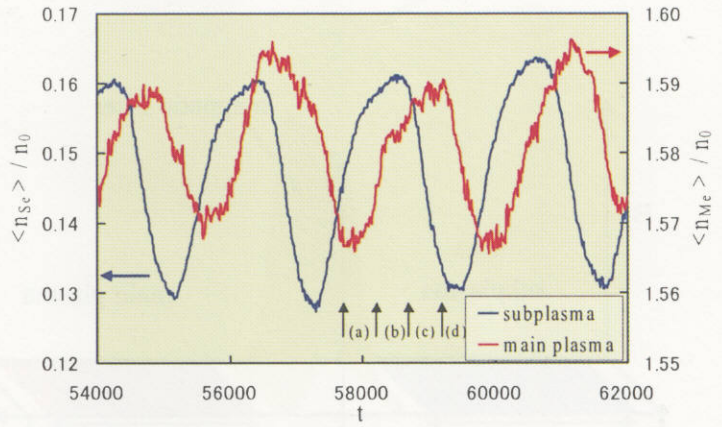

Fig. 6

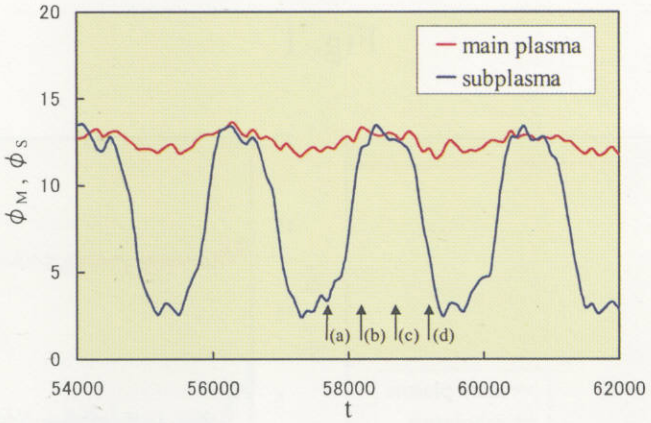

Fig. 7

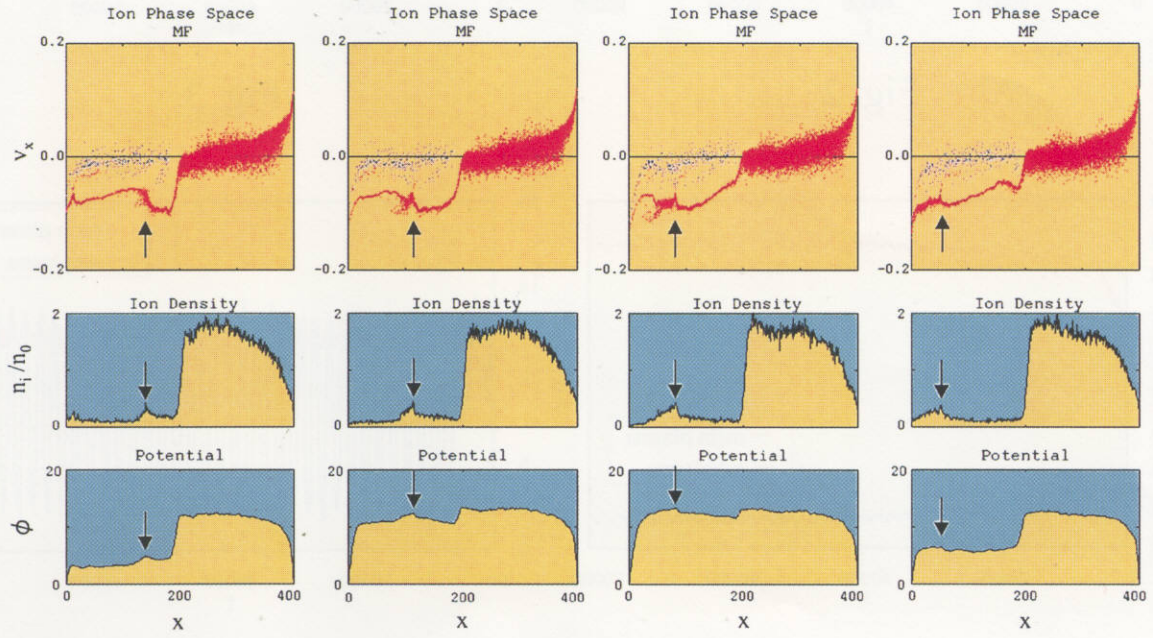

(a) t = 57700 (b) t = 58200 (c) t = 58700 (d) t = 59200

Fig. 8

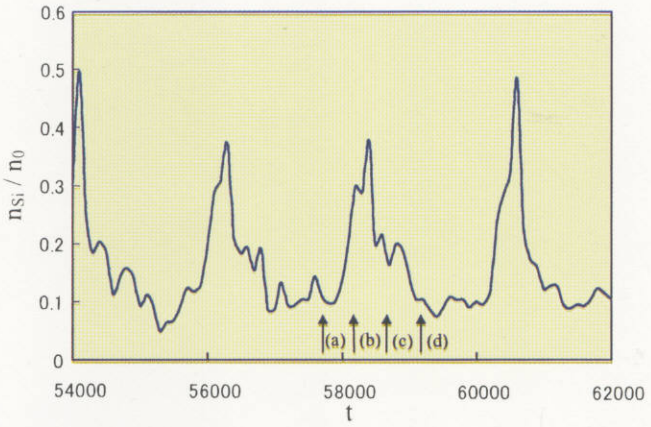

Fig. 9

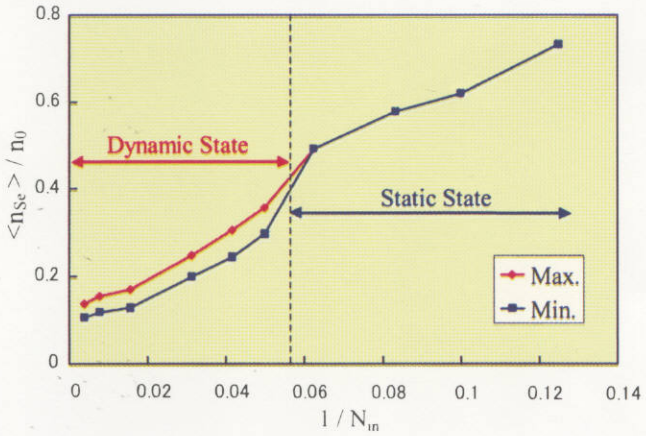

Fig. 10

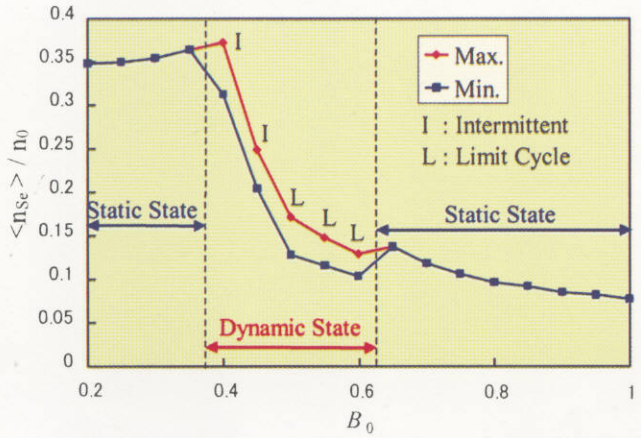

Fig. 11

Recent Issues of NIFS Series

NIFS-577 S. Fujiwara and T. Sato,
Molecular Dynamics Simulation of Structure Formation of Short Chain Molecules, Nov. 1998

NIFS-578 T. Yamagishi,
Eigenfunctions for Vlasov Equation in Multi-species Plasmas Nov. 1998

NIFS-579 M. Tanaka, A. Yu Grosberg and T. Tanaka,
Molecular Dynamics of Strongly-Coupled Multichain Coulomb Polymers in Pure and Salt Aqueous Solutions; Nov. 1998

NIFS-580 J. Chen, N. Nakajima and M. Okamoto,
Global Mode Analysis of Ideal MHD Modes in a Heliotron/Torsatron System: I. Mercier-unstable Equilibria; Dec. 1998

NIFS-581 M. Tanaka, A. Yu Grosberg and T. Tanaka,
Comparison of Multichain Coulomb Polymers in Isolated and Periodic Systems: Molecular Dynamics Study; Jan. 1999

NIFS-582 V.S. Chan and S. Murakami,
Self-Consistent Electric Field Effect on Electron Transport of ECH Plasmas; Feb. 1999

NIFS-583 M. Yokoyama, N. Nakajima, M. Okamoto, Y. Nakamura and M. Wakatani,
Roles of Bumpy Field on Collisionless Particle Confinement in Helical-Axis Heliotrons; Feb. 1999

NIFS-584 T.-H. Watanabe, T. Hayashi, T. Sato, M. Yamada and H. Ji,
Modeling of Magnetic Island Formation in Magnetic Reconnection Experiment, Feb. 1999

NIFS-585 R. Kumazawa, T. Mutoh, T. Seki, F. Shinpo, G. Nomura, T. Ido, T. Watari, Jean-Marie Noterdaeme and Yangping Zhao,
Liquid Stub Tuner for Ion Cyclotron Heating; Mar. 1999

NIFS-586 A. Sagara, M. Iima, S. Inagaki, N. Inoue, H. Suzuki, K. Tsuzuki, S. Masuzaki, J. Miyazawa, S. Morita, Y. Nakamura, N. Noda, B. Peterson, S. Sakakibara, T. Shimozuma, H. Yamada, K. Akaishi, H. Chikaraishi, H. Funaba, O. Kaneko, K. Kawahata, A. Komori, N. Ohyabu, O. Motojima, LHD Exp. Group 1, LHD Exp. Group 2,
Wall Conditioning at the Starting Phase of LHD; Mar. 1999

NIFS-587 T. Nakamura and T. Yabe,
Cubic Interpolated Propagation Scheme for Solving the Hyper-Dimensional Vlasov-Poisson Equation in Phase Space; Mar. 1999

NIFS-588 W.X. Wang, N. Nakajima, S. Murakami and M. Okamoto,
An Accurate δf Method for Neoclassical Transport Calculation, Mar. 1999

NIFS-589 K. Kishida, K. Araki, S. Kishiba and K. Suzuki,
Local or Nonlocal? Orthonormal Divergence-free Wavelet Analysis of Nonlinear Interactions in Turbulence; Mar. 1999

NIFS-590 K. Araki, K. Suzuki, K. Kishida and S. Kishiba,
Multiresolution Approximation of the Vector Fields on T^3; Mar. 1999

NIFS-591 K. Yamazaki, H. Yamada, K.Y. Watanabe, K. Nishimura, S. Yamaguchi, H. Nakanishi, A. Komori, H. Suzuki, T. Mito, H. Chikaraishi, K. Murai, O. Motojima and the LHD Group,
Overview of the Large Helical Device (LHD) Control System and Its First Operation; Apr. 1999

NIFS-592 T. Takahashi and Y. Nakao,
Thermonuclear Reactivity of D-T Fusion Plasma with Spin-Polarized Fuel, Apr. 1999

NIFS-593 H. Sugama,
Damping of Toroidal Ion Temperature Gradient Modes; Apr. 1999

NIFS-594 Xiaodong Li,
Analysis of Crowbar Action of High Voltage DC Power Supply in the LHD ICRF System; Apr. 1999

NIFS-595 K. Nishimura, R. Horiuchi and T. Sato,
Drift-kink Instability Induced by Beam Ions in Field-reversed Configurations, Apr. 1999

NIFS-596 Y. Suzuki, T-H. Watanabe, T. Sato and T. Hayashi,
Three-dimensional Simulation Study of Compact Toroid Plasmoid Injection into Magnetized Plasmas; Apr. 1999

NIFS-597 H. Sanuki, K. Itoh, M. Yokoyama, A. Fujisawa, K. Ida, S. Toda, S.-I. Itoh, M. Yagi and A. Fukuyama,
Possibility of Internal Transport Barrier Formation and Electric Field Bifurcation in LHD Plasma;
May 1999

NIFS-598 S. Nakazawa, N. Nakajima, M. Okamoto and N. Ohyabu,
One Dimensional Simulation on Stability of Detached Plasma in a Tokamak Divertor; June 1999

NIFS-599 S. Murakami, N. Nakajima, M. Okamoto and J. Nhrenberg,
Effect of Energetic Ion Loss on ICRF Heating Efficiency and Energy Confinement Time in Heliotrons;
June 1999

NIFS-600 R. Horiuchi and T. Sato,
Three-Dimensional Particle Simulation of Plasma Instabilities and Collisionless Reconnection in a Current Sheet;; June 1999

NIFS-601 W. Wang, M. Okamoto, N. Nakajima and S. Murakami,
Collisional Transport in a Plasma with Steep Gradients; June 1999

NIFS-602 T. Mutoh, R. Kumazawa, T. Saki, K. Saito, F. Simpo, G. Nomura, T. Watari, X. Jikang, G. Cattanei, H. Okada, K. Ohkubo, M. Sato, S. Kubo, T. Shimozuma, H. Idei, Y. Yoshimura, O. Kaneko, Y. Takeiri, M. Osakabe, Y. Oka, K. Tsumori, A. Komori, H. Yamada, K. Watanabe, S. Sakakibara, M. Shoji, R. Sakamoto, S. Inagaki, J. Miyazawa, S. Morita, K. Tanaka, B.J. Peterson, S. Murakami, T. Minami, S. Ohdachi, S. Kado, K. Narihara, H. Sasao, H. Suzuki, K. Kawahata, N. Ohyabu, Y. Nakamura, H. Funaba, S. Masuzaki, S. Muto, K. Sato, T. Morisaki, S. Sudo, Y. Nagayama, T. Watanabe, M. Sasao, K. Ida, N. Noda, K. Yamazaki, K. Akaishi, A. Sagara, K. Nishimura, T. Ozaki, K. Toi, O. Motojima, M. Fujiwara, A. Iiyoshi and LHD Exp. Group 1 and 2,
First ICRF Heating Experiment in the Large Helical Device; July 1999

NIFS-603 P.C. de Vries, Y. Nagayama, K. Kawahata, S. Inagaki, H. Sasao and K. Nagasaki,
Polarization of Electron Cyclotron Emission Spectra in LHD; July 1999

NIFS-604 W. Wang, N. Nakajima, M. Okamoto and S. Murakami,
δf Simulation of Ion Neoclassical Transport; July 1999

NIFS-605 T. Hayashi, N. Mizuguchi, T. Sato and the Complexity Simulation Group,
Numerical Simulation of Internal Reconnection Event in Spherical Tokamak; July 1999

NIFS-606 M. Okamoto, N. Nakajima and W. Wang,
On the Two Weighting Scheme for δf Collisional Transport Simulation; Aug. 1999

NIFS-607 O. Motojima, A.A. Shishkin, S. Inagaki, K.Y. Watanabe,
Possible Control Scenario of Radial Electric Field by Loss-Cone-Particle Injection into Helical Device; Aug. 1999

NIFS-608 R. Tanaka, T. Nakamura and T. Yabe,

Constructing Exactly Conservative Scheme in Non-conservative Form, Aug 1999

NIFS-609 H. Sugama,
Gyrokinetic Field Theory, Aug 1999

NIFS-610 M. Takechi, G. Matsunaga, S. Takagi, K. Ohkuni, K. Toi, M. Osakabe, M. Isobe, S. Okamura, K. Matsuoka, A. Fujisawa, H. Iguchi, S. Lee, T. Minami, K. Tanaka, Y. Yoshimura and CHS Group,
Core Localized Toroidal Alfven Eigenmodes Destabilized By Energetic Ions in the CHS Heliotron/Torsatron, Sep 1999

NIFS-611 K. Ichiguchi,
MHD Equilibrium and Stability in Heliotron Plasmas; Sep 1999

NIFS-612 Y. Sato, M. Yokoyama, M. Wakatani and V. D. Pusovitov,
Complete Suppression of Pfirsch-Schluter Current in a Toroidal l=3 Stellarator, Oct. 1999

NIFS-613 S. Wang, H. Sanuki and H. Sugama,
Reduced Drift Kinetic Equation for Neoclassical Transport of Helical Plasmas in Ultra-low Collisionality Regime, Oct. 1999

NIFS-614 J. Miyazawa, H. Yamada, K. Yasui, S. Kato, N., Fukumoto, M. Nagata and T. Uyama,
Design of Spheromak Injector Using Conical Accelerator for Large Helical Device; Nov 1999

NIFS-615 M. Uchida, A. Fukuyama, K. Itoh, S.-I. Itoh and M. Yagi,
Analysis of Current Diffusive Ballooning Mode in Tokamaks; Dec. 1999

NIFS-616 M. Tanaka, A.Yu. Grosberg and T. Tanaka,
Condensation and Swelling Behavior of Randomly Charged Multichain Polymers by Molecular Dynamics Simulations; Dec. 1999

NIFS-617 S. Goto and S. Kida,
Sparseness of Nonlinear Coupling; Dec. 1999

NIFS-618 M.M. Skoric, T. Sato, A. Maluckov and M.S. Jovanovic,
Complexity in Laser Plasma Instabilities Dec. 1999

NIFS-619 T.-H. Watanabe, H. Sugama and T. Sato,
Non-dissipative Kinetic Simulation and Analytical Solution of Three-mode Equations of Ion Temperature Gradient Instability, Dec 1999

NIFS-620 Y. Oka, Y. Takeiri, Yu.I.Belchenko, M. Hamabe, O. Kaneko, K. Tsumori, M. Osakabe, E. Asano, T. Kawamoto, R. Akiyama,
Optimization of Cs Deposition in the 1/3 Scale Hydrogen Negative Ion Source for LHD-NBI System ; Dec. 1999

NIFS-621 Yu.I. Belchenko, Y. Oka, O. Kaneko, Y. Takeiri, A. Krivenko, M. Osakabe, K. Tsumori, E. Asano, T. Kawamoto, R. Akiyama,
Recovery of Cesium in the Hydrogen Negative Ion Sources; Dec 1999

NIFS-622 Y. Oka, O. Kaneko, K. Tsumori, Y. Takeiri, M. Osakabe, T. Kawamoto, E. Asano, and R. Akiyama,
H- Ion Source Using a Localized Virtual Magnetic Filter in the Plasma Electrode: Type I LV Magnetic Filter: Dec. 1999

NIFS-623 M. Tanaka, S. Kida, S. Yanase and G. Kawahara,
Zero-absolute-vorticity State in a Rotating Turbulent Shear Flow; Jan 2000

NIFS-624 F. Leuterer, S. Kubo,
Electron Cyclotron Current Drive at $\omega \approx \omega_c$ with X-mode Launched from the Low Field Side; Feb. 2000

NIFS-625 K. Nishimura,
Wakefield of a Charged Particulate Influenced by Emission Process of Secondary Electrons; Mar. 2000

NIFS-626 K. Itoh, M. Yagi, S.-I. Itoh, A. Fukuyama,
On Turbulent Transport in Burning Plasmas; Mar. 2000

NIFS-627 K. Itoh, S.-I. Itoh, L. Giannone,
Modelling of Density Limit Phenomena in Toroidal Helical Plasmas; Mar. 2000

NIFS-628 K. Akaishi, M. Nakasuga and Y. Funato,
True and Measured Outgassing Rates of a Vacuum Chamber with a Reversibly Absorbed Phase; Mar 2000

NIFS-629 T. Yamagishi,
Effect of Weak Dissipation on a Drift Orbit Mapping; Mar. 2000

NIFS-630 S. Toda, S.-I, Itoh, M. Yagi, A. Fukuyama and K. Itoh,
Spatial Structure of Compound Dither in L/H Transition; Mar. 2000

NIFS-631 N. Ishihara and S. Kida,
Axial and Equatorial Magnetic Dipoles Generated in a Rotating Spherical Shell; Mar. 2000

NIFS-632 T. Kuroda, H. Sugama, R. Kanno and M. Okamoto,
Ion Temperature Gradient Modes in Toroidal Helical Systems; Apr. 2000

NIFS-633 V.D. Pustovitov,
Magnetic Diagnostics: General Principles and the Problem of Reconstruction of Plasma Current and Pressure Profiles in Toroidal Systems, Apr 2000

NIFS-634 A.B. Mikhailovskii, S.V Konovalov, V.D Pustovitov and V.S Tsypin,
Mechanism of Viscosity Effect on Magnetic Island Rotation; Apr. 2000

NIFS-635 H. Naitou, T. Kuramoto, T. Kobayashi, M. Yagi, S. Tokuda and T. Matsumoto,
Stabilization of Kinetic Internal Kink Mode by Ion Diamagnetic Effects; Apr. 2000

NIFS-636 A. Kageyama and S. Kida,
A Spectral Method in Spherical Coordinates with Coordinate Singularity at the Origin; Apr. 2000

NIFS-637 R. Horiuchi, W. Pei and T. Sato,
Collisionless Driven Reconnection in an Open System; June 2000

NIFS-638 K. Nagaoka, A. Okamoto, S. Yoshimura and M.Y. Tanaka,
Plasma Flow Measurement Using Directional Langmuir Probe under Weakly Ion-Magnetized Conditions; July 2000

NIFS-639 Alexei Ivanov,
Scaling of the Distribution Function and the Critical Exponents near the Point of a Marginal Stability under the Vlasov-Poisson Equations; Aug. 2000

NIFS-640 K. Ohi, H. Naitou, Y. Tauchi, O Fukumasa,
Observation of the Limit Cycle in the Asymmetric Plasma Divided by the Magnetic Filter; Aug. 2000